Title

Effect of wash media type during PBMC isolation on downstream characterization of SARS-CoV-2-specific T cells.

Authors

Congrave-Wilson, Zion
Kim, Minjun
Sutherland, Aaron
et al.

Publication Date

2023-08-01

DOI

10.1016/j.jim.2023.113520

Peer reviewed

Since January 2020 Elsevier has created a COVID-19 resource centre with free information in English and Mandarin on the novel coronavirus COVID-19. The COVID-19 resource centre is hosted on Elsevier Connect, the company's public news and information website.

Effect of wash media type during PBMC isolation on downstream characterization of SARS-CoV-2-specific T cells

Zion Congrave-Wilson, Minjun Kim, Aaron Sutherland, Jaycee Jumarang, Yesun Lee, Jennifer Del Valle, Wesley A. Cheng, Ricardo Da Silva Antunes, Pia S. Pannaraj

PII: S0022-1759(23)00102-3

DOI: https://doi.org/10.1016/j.jim.2023.113520

Reference: JIM 113520

To appear in: *Journal of Immunological Methods*

Received date: 19 March 2023

Revised date: 13 June 2023

Accepted date: 27 June 2023

Please cite this article as: Z. Congrave-Wilson, M. Kim, A. Sutherland, et al., Effect of wash media type during PBMC isolation on downstream characterization of SARS-CoV-2-specific T cells, *Journal of Immunological Methods* (2023), https://doi.org/10.1016/j.jim.2023.113520

Effect of Wash Media Type during PBMC Isolation on Downstream Characterization of SARS-CoV-2-Specific T Cells

Zion Congrave-Wilson, MSc[1], Minjun Kim, BA[1], Aaron Sutherland, BS[2], Jaycee Jumarang, MD[1], Yesun Lee, PhD[1], Jennifer Del Valle, BS[1], Wesley A. Cheng, BS[1], Ricardo Da Silva Antunes, PhD[2], Pia S. Pannaraj, MD, MPH[1,3,*]

[1]Division of Infectious Diseases, Children's Hospital Los Angeles, Los Angeles, CA, United States

[2]Center for Infectious Disease and Vaccine Research, La Jolla Institute for Immunology, La Jolla, CA, United States

[3]Department of Pediatrics and Molecular Microbiology and Immunology, Keck School of Medicine, University of Southern California, Los Angeles, CA, United States

**Corresponding Author:*

Pia S. Pannaraj, MD, MPH

Associate Professor, Pediatrics and Molecular Microbiology and Immunology

Keck School of Medicine, University of Southern California

Children's Hospital Los Angeles

4650 Sunset Blvd., MS #51, Los Angeles, CA 90027

Email: ppannaraj@chla.usc.edu, Telephone: 323-361-2509, Fax: 323-361-1183

Abstract

Protocols for the isolation of peripheral blood mononuclear cells (PBMCs) from whole blood vary greatly between laboratories, especially in published studies of SARS-CoV-2-specific T cell responses following infection and vaccination. Research on the effects of different wash media types or centrifugation speeds and brake usage during the PBMC isolation process on downstream T cell activation and functionality is limited. Blood samples from 26 COVID-19-vaccinated participants were processed with different PBMC isolation methods using either PBS or RPMI as the wash media with high centrifugation speed and brakes or RPMI as the wash media with low speed and brakes (RPMI+ method). SARS-CoV-2 spike-specific T cells were quantified and characterized via a flow cytometry-based activation induced markers (AIM) assay and an interferon-γ (IFNγ) FluoroSpot assay and responses were compared between processing methods. Samples washed with RPMI showed higher AIM^+ CD4 T cell responses than those washed with PBS and showed a shift away from naïve and towards an effector memory phenotype. The activation marker OX40 showed higher SARS-CoV-2 spike-induced upregulation on RPMI-washed CD4 T cells, while differences in CD137 upregulation were minimal between processing methods. The magnitude of the AIM^+ CD8 T cell response was similar between processing methods but showed higher stimulation indices. Background frequencies of $CD69^+$ CD3 T cells were increased in PBS-washed samples and were associated with higher baseline numbers of IFNγ-producing cells in the FluoroSpot assay. Slower braking in the RPMI+ method did not improve detection of SARS-CoV-2-specific T cells and caused longer processing times. Thus, the use of RPMI media with full centrifugation brakes during the wash steps of PBMC isolation was found to be most effective and efficient. Further studies are needed to elucidate the pathways involved in RPMI-mediated preservation of downstream T cell activity.

Keywords: T cell, processing, wash media, centrifugation brakes, flow cytometry, FluoroSpot

Abbreviations

AIM – Activation induced markers

CHLA – Children's Hospital Los Angeles

COVID-19 – Coronavirus disease 2019

DMSO – Dimethyl sulfoxide

EDTA – Ethylenediaminetetraacetic acid

ELISpot – Enzyme-linked immunosorbent spot

FACS – Fluorescence-activated cell sorting

HEPES – N-2-hydroxyethylpiperazine-N-2-ethane sulfonic acid

HLA – Human leukocyte antigen

IFNγ – Interferon-γ

IQR – Interquartile range

MP – Megapool

PBMC – Peripheral blood mononuclear cell

PBS – Phosphate-buffered saline

PHA – Phytohemagglutinin-L

PVDF – Polyvinylidene difluoride

RPMI – Roswell Park Memorial Institute 1640 medium

RT-PCR – Reverse transcription polymerase chain reaction

SARS-CoV-2 – Severe acute respiratory syndrome coronavirus 2

SFC – Spot forming cells

SI – Stimulation index

T_{CM} cell – Central memory T cell

T_{EM} cell – Effector memory T cell

T_{EMRA} cell – Terminally differentiated effector memory T cell

T_N cell – Naïve T cell

1. Introduction

Throughout the COVID-19 pandemic, researchers have quantified and characterized T cell responses to SARS-CoV-2 infection and COVID-19 vaccination using a variety of methods, including ELISpot and FluoroSpot assays (Naranbhai et al., 2022; Tarke et al., 2021) and the agnostic activation induced marker (AIM) assay (Dan et al., 2021; Goel et al., 2021; Painter et al., 2021). These techniques require the maintenance of T cell functionality and viability during lymphocyte isolation from whole blood in order to differentiate SARS-CoV-2-specific cells from background populations. Detection of rare antigen-specific T cell populations can be further improved by minimizing baseline T cell activation. Over a decade ago, a T cell workshop committee reviewed the literature to identify practices during peripheral blood mononuclear cell (PBMC) isolation that were most beneficial for detection of rare antigen-specific T cell populations, specifically to improve detection of islet-specific T cells for type I diabetes research. The authors of the review found limited data on the effects of different wash media, or centrifugation speed and brake usage, during the isolation process on downstream T cell activation and functionality (Mallone et al., 2011)., To our knowledge, no studies have filled this gap in the literature in the years since the review's publication.

During the PBMC isolation process, researchers report using a range of media during the wash steps; the most commonly used are RPMI-1640 medium (RPMI) and phosphate buffered saline (PBS) solution (Gautam et al., 2019; Protocol No. DMID-OCRR-SOP-002, 2021; Rydyznski Moderbacher et al., 2020). Centrifugation speeds and brake usage during PBMC isolation also vary considerably between protocols from different laboratories (Higdon et al., 2016; Kemp et al., 2020; Protocol No. DMID-OCRR-SOP-002, 2021). Here, we processed PBMC samples from COVID-19 vaccinated individuals using either PBS or RPMI as the wash media and using two different centrifugation speeds and brake settings. We compared downstream T cell activity using a flow cytometry-based AIM assay that quantified and characterized SARS-CoV-2-specific CD4 and CD8 T cells. We also compared the effect of

processing method on the individual upregulation of activation markers OX40, CD69, and CD137 on T cells following stimulation with the SARS-CoV-2 spike protein. Lastly, a FluoroSpot assay was used to compare SARS-CoV-2-induced expansion of interferon-γ (IFNγ)-producing cells in a subset of samples. Our data provides a side-by-side comparison of different wash media types and centrifugation speed and brake settings for improving T cell performance in functional assays to aid in the identification of rare antigen-specific populations.

2. Methods

2.1 Study participants and specimen collection

All participants (Table 1) were enrolled in a Normal Donor study for assay optimization at Children's Hospital Los Angeles (CHLA) through a convenience recruitment strategy and by word of mouth. Basic demographic information, COVID-19 vaccination, and RT-PCR-confirmed SARS-CoV-2 infection history were taken at enrollment. Written consent was obtained from all participants, and the study was approved by the institutional review board of CHLA (CHLA-18-00098).

Blood was collected from participants between August and December 2022 by trained clinical research staff at CHLA's drive-thru collection center. A total of 40 to 60 mL blood was collected from each participant in ethylenediaminetetraacetic acid (EDTA) tubes. Blood samples were transported to the laboratory and processed within 2 hours after collection.

2.2 PBMC processing methods

Three PBMC isolation methods were compared in the present study; they are referred to as the "PBS," "RPMI," and "RPMI+" methods and their differences are outlined in Table 2.

2.2.1 PBS method

For the PBS method, blood samples in EDTA tubes were centrifuged in a Sorvall Legend X1R centrifuge (ThermoFisher Scientific, Waltham, MA, USA) for 10 minutes at 1200xG and at maximum acceleration and deceleration settings (acceleration: 9; deceleration: 9). The

top plasma layer was removed and stored, and the remaining blood was reconstituted to the original volume with phosphate buffered saline, pH 7.4 (PBS) (Gibco, ThermoFisher Scientific, Waltham, MA, USA). The tubes were then gently mixed by inversion, and the blood was transferred to Leucosep tubes (Greiner Bio-One, Kremsmünster, Austria) for centrifugation at 1000xG for 10 minutes, without brakes (deceleration: 0). The PBMC buffy coat was transferred into a sterile 50 mL conical tube, and the cells were washed twice in 35 mL PBS using a centrifugation setting of 400xG for 10 minutes at maximum deceleration. Then, the cells were resuspended in 20 mL PBS for cell counting using an automated cell counter (DeNovix, Wilmington, DE, USA) and spun down for 10 minutes at 400xG and maximum deceleration.

2.2.2 RPMI method

For the RPMI method, all steps were the same as the PBS method except that the blood reconstitution and PBMC wash steps used RPMI-1640 medium + 2.05 mM L-glutamine (Cytiva, Marlborough, MA, USA) instead of PBS.

2.2.3 RPMI+ method

For the RPMI+ method, the reconstitution and wash steps were also performed with RPMI-1640 medium, but at lower centrifugation speeds and deceleration settings. Briefly, whole blood was centrifuged for 10 minutes at 800xG, without brakes, for the initial plasma separation step. Then, blood diluted in a 2:1 ratio of RPMI to the original volume and was overlaid on Ficoll-Paque Plus (Cytiva, Marlborough, MA, USA). The PBMC buffy coat separation spin was for 25 minutes at 800xG, without brakes. After isolation of the buffy coat, cells were washed once with 35 mL RPMI and centrifuged for 10 minutes at 400xG, low brakes (deceleration: 4) before resuspension in 20 mL RPMI for cell counting. The final centrifugation spin before freezing was at 200xG for 10 minutes, no brakes.

2.2.4 Cryopreservation

For storage, all PBMC samples were resuspended in 10% dimethyl sulfoxide (DMSO) (VWR International, Radnor, PA, USA) in heat inactivated fetal bovine serum (Genesee

Scientific, San Diego, CA, USA) at a concentration of at least $5x10^6$ cells/mL and aliquoted to cryovials. Cryovials were immediately moved to –80˚C freezers for step-down freezing at -1˚C/minute in a Mr. Frosty isopropyl alcohol cell cooler (ThermoFisher Scientific, Waltham, MA, USA) for at least 24 hours before moving to liquid nitrogen for storage.

2.3 SARS-CoV-2 activation induced markers (AIM) T cell assay

An AIM T cell assay was used for detection of SARS-CoV-2 spike-specific T cells (Dan et al., 2021). Briefly, PBMCs were thawed and resuspended in HR5 medium (RPMI-1640 + 25 mM HEPES [Gibco, ThermoFisher Scientific, Waltham, MA, USA] supplemented with 5% human AB serum [GeminiBio, Sacramento, CA, USA], 1% GlutaMAX [ThermoFisher Scientific, Waltham, MA, USA], and 200 mM Penicillin/Streptomycin [Sigma-Aldritch, St. Louis, MO, USA]) containing 20 units/mL benzonase nuclease [MilliporeSigma, Burlington, MA, USA]). Cells were seeded into a microtiter plate at $1x10^6$ cells per well and rested overnight in HR5 medium at 37°C and 5% CO_2. Then, cells were stimulated for 23-24 hours with either 1 µg/mL DMSO, 1 µg/mL spike megapool (Spike MP, kindly provided by La Jolla Institute for Immunology), or 10 µg/mL phytohemagglutinin-L (PHA) (MilliporeSigma, Burlington, MA, USA) in HR5 medium. Spike MP is a peptide pool that contains overlapping 15-mer peptides spanning the entire SARS-CoV-2 spike protein. After stimulation, cells were stained with 1:100 Zombie UV viability dye (BioLegend, San Diego, CA, USA) in PBS followed by the antibody cocktail presented in Supplementary Table 1. Cells were then resuspended in FACS Buffer (2% FBS, 0.1% sodium azide in PBS) and analyzed using a BD LSR II flow cytometer (BD Biosciences, San Diego, CA, USA). Compensation beads were included for each run. All analyses were performed using the FlowJo software version 10.8.1 (BD Biosciences, San Diego, CA, USA).

Gating strategies for CD4 and CD8 T cells can be found in Supplementary Fig. 1A. AIM^+ CD4 and CD8 T cells were defined as CD134 $(OX40)^+CD137^+$ (Supplementary Fig. 1B) and $CD69^+CD137^+$ (Supplementary Fig. 1D), respectively. Classification of memory subsets was determined by CCR7 and CD45RA staining ($CD45RA^+CCR7^+$, naïve [T_N]; $CD45RA^-CCR7^+$,

central memory [T_{CM}]; $CD45RA^{-}CCR7^{-}$, effector memory [T_{EM}]; $CD45RA^{+}CCR7^{-}$, terminally differentiated effector memory [T_{EMRA}]) for both CD4 and CD8 T cells (Supplementary Fig. 1C,E). Memory phenotyping was performed on samples with a Spike MP AIM^{+} T cell stimulation index greater than 2. Gating strategies for AIM^{+} CD4 and AIM^{+} CD8 T cells, single OX40, CD69, and CD137 expression, and memory subsets were determined using fluorescence minus one controls. All samples showed sufficient PHA-stimulated polyclonal expansion, defined as over 10% AIM^{+} CD4 or CD8 T cells, for at least one processing method.

2.4 SARS-CoV-2 interferon-γ (IFNγ) FluoroSpot assay

An IFNγ FluoroSpot assay was additionally used for detection of SARS-CoV-2-specific T cells (Mateus et al., 2020). Briefly, PVDF membrane FluoroSpot plates (Mabtech, Stockholm, Sweden) were coated with 5 µg/mL coating antibody in PBS (anti-IFNγ [clone: 1-D1K]; Mabtech, Stockholm, Sweden) overnight at 4˚C. PBMCs were thawed and resuspended in HR5 medium supplemented with 20 units/mL benzonase nuclease. Cells were counted and seeded into a microtiter plate at $2.5x10^{5}$ cells per well where cells were stimulated with either 1 µg/mL DMSO, 1 µg/mL Spike MP, or 10 µg/mL PHA in HR5 medium for 23-24 hours. All stimulations were performed in triplicate. After stimulation, plates were washed with PBS-0.05% Tween20 (Sigma-Aldrich, St. Louis, MO, USA) and incubated for 2 hours at room temperature with detection antibody (anti-IFNγ-BAM [clone: 7-B6-1]; Mabtech, Stockholm, Sweden) in PBS-0.1% bovine serum albumin (Rockland Immunochemicals, Gilbertsville, PA, USA). The plates were washed again and incubated for 1 hour in the dark with the fluorophore-conjugated antibody solution (anti-BAM-490; Mabtech, Stockholm, Sweden). Plates were read by a Mabtech IRIS FluoroSpot reader (Mabtech, Stockholm, Sweden). Responses are reported as the average number of spot forming cells (SFC)/10^{6} PBMC from the triplicate.

2.5 Statistics

The magnitude of the spike-specific T cell response is reported as the difference between the proportions of AIM^{+} CD4 or CD8 T cells (AIM assay) or numbers of SFC/10^{6} PBMC

(FluoroSpot assay) in the Spike MP-stimulated condition and the DMSO-stimulated condition. The stimulation index (SI) is defined as the fold change in the proportion of AIM^+ T cells or $SFC/10^6$ PBMC in the stimulated condition over the DMSO condition. Comparisons between paired samples for each processing method were computed using the Wilcoxon signed-rank test. Correlations were calculated by Spearman's correlation coefficient. All statistical tests were performed using GraphPad Prism version 9 (San Diego, CA, USA) with a two-tailed p-value <0.05 considered significant.

3. Results

3.1 Study participants and demographics

One blood sample was collected from each of 26 participants following COVID-19 vaccination. At each collection, blood samples from the same participant were split into equal volumes and processed according to either the PBS, RPMI, or RPMI+ processing method. Blood from two participants was processed using only two methods due to small blood collection volumes; all other participants had sufficient blood volumes to allow for all three processing methods.

The participants' demographic information can be found in Table 1. All participants received at least the primary series of a COVID-19 vaccine. Most participants (92.3%) reported receiving an mRNA vaccine for their primary series and booster. The two participants who reported receiving Ad26.COV2.S for their primary series received an mRNA vaccine as a booster dose. One participant had completed only an mRNA vaccine primary series at the time of blood collection and had not yet received a booster dose. Two participants received the bivalent mRNA-1273.214 vaccine as a booster dose. The median time since last vaccine dose for all participants was 277 days (IQR: 244-338 days). Half of the participants reported at least one previous SARS-CoV-2 infection, and the median time since last infection was 233 days (IQR: 65-316 days) for convalescent participants.

3.2 Spike-specific CD4 T cell responses by processing method

We compared CD4 T cell responses to the SARS-CoV-2 spike protein between PBMC samples processed using the PBS, RPMI, and RPMI+ methods by the flow cytometry-based AIM assay (Fig. 1A). The frequency of background AIM^+ CD4 T cells did not significantly differ between processing methods (Fig. 1B). Following PHA stimulation, RPMI+-processed samples showed significantly lower frequencies of AIM^+ CD4 T cells than PBS- or RPMI-processed samples (median % AIM^+ of total CD4 T cells, RPMI+ [24.1%] vs. PBS [29.4%] and RPMI [28.7%], both p=0.034; Fig. 1C).

The magnitude of spike-specific CD4 T cell responses was either significantly higher or trended higher in samples processed using the RPMI method compared with the other methods (median spike-specific CD4 T cell magnitude, RPMI [0.13%] vs. PBS [0.10%] and RPMI+ [0.11%], p=0.020 and p=0.05, respectively; Fig. 1D). However, there were no observable differences in the stimulation indices of AIM^+ CD4 T cells when comparing between the processing methods (median AIM^+ CD4 T cell stimulation index, PBS [23.3] vs. RPMI [26.5] vs. RPMI+ [26.6], all p>0.10; Fig. 1E). We then checked whether the processing method shifted the phenotypic composition of these antigen-specific populations (Fig. 1F). Both RPMI- and RPMI+-processed samples were associated with lower proportions of T_N cells compared with PBS-processed samples (median % T_N of AIM^+ CD4, RPMI [15.5%] and RPMI+ [14.6%] vs. PBS [22.6%], p=0.038 and p=0.007, respectively; Fig 1G). This reduction corresponded with a significant increase in the proportion of T_{EM} cells for RPMI-processed samples, which also trended higher for RPMI+-processed samples (median % T_{EM} of AIM^+ CD4, RPMI [47.8%] and RPMI+ [43.7%] vs. PBS [35.5%], p=0.011 and p=0.10, respectively).

As an alternative analysis, differences in the individual upregulation of the activation markers OX40 or CD137 on CD4 T cells were considered between processing methods (Fig. 2A-B). Stimulation with the Spike MP induced significantly higher OX40 expression in both RPMI- and RPMI+-processed samples compared to PBS-processed samples (median spike-

specific $OX40^+$ CD4 magnitude, RPMI [0.79%] and RPMI+ [0.76%] vs. PBS [0.52%], p=0.024 and p=0.027, respectively; Fig. 2E). Stimulation indices also trended higher and were higher for RPMI- and RPMI+-processed samples over PBS-processed samples (median $OX40^+$ CD4 stimulation index, RPMI [22.3] and RPMI+ [27.7] vs. PBS [11.3], p=0.10 and p=0.008, respectively; Fig. 2F). In contrast, the differences in the upregulation of CD137 on CD4 T cells between processing methods were relatively minor (Fig. 2G-J).

3.3 Spike-specific CD8 T cell responses by processing method

SARS-CoV-2 spike-specific CD8 T cells were also identified by the AIM assay and compared between the different processing methods (Fig. 3A). As expected, we observed higher background frequencies of AIM^+ CD8 T cells than AIM^+ CD4 T cells, but background AIM^+ CD8 levels did not significantly differ between processing methods (Fig. 3B). Frequencies of AIM^+ CD8 T cells in PHA-stimulated polyclonal expansions were also similar between processing methods, except that RPMI-processed samples showed slightly higher signal compared with PBS-processed samples (median % AIM^+ of total CD8, RPMI [61.2%] vs. PBS [54.7%], p=0.036; Fig. 3C).

Spike-specific CD8 T cell responses were highly variable between individuals and did not show any significant difference in magnitude between the processing methods (Fig. 3D). However, RPMI- and RPMI+-processed samples trended higher and showed significantly higher stimulation indices for AIM^+ CD8 T cells, respectively, compared to PBS-processed samples (median AIM^+ CD8 stimulation index, RPMI [9.2] and RPMI+ [9.8] vs. PBS [4.4], p=0.07 and p=0.029, respectively; Fig. 3E). Spike-specific CD8 T cell responses were further characterized by looking at the memory compartments (Fig. 3F). These populations did not show a noticeable shift in phenotype between processing methods, except for a slight reduction in T_{CM} cells in RPMI+-processed samples compared with PBS-processed samples (median % T_{CM} of AIM^+ CD8, RPMI+ [0.5%] vs. PBS [1.1%], p=0.031; Fig. 3G). However, these comparisons were less

powered than for AIM^+ CD4 as many PBS-processed samples had AIM^+ CD8 responses that were under an SI of 2.

An alternative analysis was performed for AIM^+ CD8 T cells to examine differences in the individual upregulation of the activation markers CD69 and CD137 by processing method (Fig. 4A-B). Background CD69 expression was significantly lower in RPMI- and RPMI+-processed samples compared with PBS-processed samples (median % $CD69^+$ of total CD8, RPMI [6.8%] and RPMI+ [6.3%] vs. PBS [10.1%], p=0.018 and p=0.008, respectively; Fig. 4C). The magnitude of CD69 upregulation on CD8 T cells following Spike MP stimulation was significantly higher in RPMI+ samples compared with PBS samples (median spike-specific $CD69^+$ CD8 magnitude, RPMI+ [4.7%] vs. PBS [3.0%], p=0.049; Fig. 4E). Lower background expression in RPMI- and RPMI+-processed samples resulted in increased stimulation indices for CD69 expression on CD8 T cells, although high baseline expression made these indices small across the groups (median $CD69^+$ CD8 stimulation index, RPMI [2.0] and RPMI+ [2.2] vs. PBS [1.4], p=0.010 and p=0.024, respectively; Fig. 4F). Similar to CD4 T cells, both background and Spike MP-induced CD137 expression on CD8 T cells did not significantly differ between processing methods (Fig. 4G, I). However, PHA-stimulated CD137 expression on CD8 T cells was significantly higher in RPMI- and RPMI+-processed samples compared with PBS-processed samples (median % $CD137^+$ of total CD8, RPMI [69.1%] and RPMI+ [66.8%] vs. PBS [61.7%], p=0.017 and p=0.036, respectively; Fig. 4H). Additionally, simulation indices of Spike MP-stimulated CD137 expression were significantly higher in RPMI+-processed compared with PBS-processed CD8 T cells (median $CD137^+$ CD8 stimulation index, RPMI+ [5.8] vs. PBS [3.6], p=0.039; Fig. 4J).

3.4 Spike-specific IFNγ-producing T cell responses by processing method

For 19 participants, we assessed functionality of spike-specific T cells using an IFNγ FluoroSpot assay, as previously described (Tarke et al., 2021), and compared their responses between processing methods (Fig. 5A). Lymphocytes processed by both the RPMI and RPMI+

methods showed significantly lower background production of IFNγ compared with PBS-processed cells (median SFC/10^6 PBMC, RPMI [3.98] and RPMI+ [2.98] vs. PBS [88.9], p=0.010 and p=0.003, respectively; Fig. 5B). The numbers of IFNγ-producing cells expanded by PHA stimulation were relatively similar between methods, although the RPMI method trended slightly higher compared to the PBS and RPMI+ methods (median SFC/10^6 PBMC, RPMI [4830] vs. PBS [4271] and RPMI+ [4430], both p=0.07; Fig. 5C). The Spike MP induced highly variable numbers of IFNγ-producing cells between participants, and we did not observe a significant difference in either the magnitude or the stimulation index of Spike MP-stimulated samples by processing method (Fig. 5D-E).

We calculated the Spearman's correlation coefficient between the baseline number of IFNγ-producing cells and background $CD69^+$ expression on CD8 T cells in the DMSO-stimulated samples from 19 participants for which both assays were run. We found a moderate correlation between the background frequency of $CD69^+$ CD8 T cells and the baseline number of IFNγ-producing cells when all processing methods were analyzed together (ρ=0.30, p=0.025; Supplementary Fig. 2A). The association was even stronger when considering only PBS-processed samples (ρ=0.74, p<0.001; Supplementary Fig. 2B); this is likely due to the greater variation in background CD8 T cell activation and FluoroSpot results for PBS-processed samples over those processed with RPMI.

4. Discussion

The variation in T cell assay protocols between laboratories prompted the creation of the Minimal Information About T Cell Assays (MIATA) project, which provides recommendations on the minimum amount of information needed in order to objectively compare immunological data between research groups (Janetzki et al., 2009). Still, some variables in the PBMC isolation process, namely the use of different wash medias and the differences in centrifugation speed and brakes, are understudied in their effect on downstream T cell assays (Mallone et al., 2011).

Investigations on the effect of these variables can improve the reproducibility of T cell assays and help researchers interpret the quality of cellular immunity studies.

While fresh PBMC samples are known to retain better viability and display less spontaneous cytokine secretion and baseline activation over frozen PBMCs (Mallone et al., 2011), we used frozen PBMC samples to provide guidance to researchers conducting studies where the use of fresh PBMCs in T cell assays may be impractical. Here, we demonstrate that use of RPMI wash media during PBMC isolation prior to freezing improved sensitivity for detecting SARS-CoV-2 spike-specific T cell populations and lowered background T cell activation. Importantly, the magnitude of the spike-specific CD4 T cell response was maximized when RPMI wash media was used instead of PBS, although the overall change in frequencies of AIM^+ CD4 T cells was relatively minor. Conversely, for spike-specific CD8 T cells, we observed no difference in the magnitude of the response between processing methods, but stimulation indices were greatest after RPMI washing. Interestingly, spike-specific CD4 T cell populations also showed a shift from cells with a naïve phenotype to an effector memory phenotype. As COVID-19 vaccine-induced responses have been observed to be primarily of the T_{CM} and T_{EM} phenotypes in CD4 T cells (Painter et al., 2021; Tarke et al., 2021), our data suggests that RPMI-washed samples showed increased sensitivity for detecting this vaccine-elicited population. This contrasts with PBS-washed samples, where activated CD4 T cells following spike stimulation showed a higher antigen-naïve phenotype, possibly reflecting unspecific bystander activation.

RPMI wash media likely improves detection of antigen-specific T cell responses and reduces background activation due to the presence of nutrients. RPMI is composed of glucose, amino acids (with the highest concentrations being L-arginine and L-glutamine), vitamins, inorganic salts, phenol red, and may be supplemented with additional L-glutamine (Cytiva, 2020). Two major nutritional differences between RPMI and PBS that are well studied for their role in T cell metabolism are glucose and glutamine (Hope and Salmond, 2021; van der Windt

and Pearce, 2012). Following antigen stimulation, T cells switch their metabolism from oxidative phosphorylation to lactate fermentation to prioritize macromolecule synthesis in a phenomenon known as the Warburg effect (van der Windt and Pearce, 2012; Wasinski et al., 2014). Glucose and glutamine fuel this metabolic shift through the glycolysis and glutaminolysis pathways, respectively (Carr et al., 2010; Palmer et al., 2015). However, glycolysis and glutaminolysis also power oxidative phosphorylation and ATP production in resting T cells, signifying the crucial role of these two molecules in T cell survival and homeostasis in addition to activation (Jacobs, 2009; Newsholme, 2001; van der Windt and Pearce, 2012). As such, the absence of glucose and glutamine in PBS washes during PBMC isolation may stress lymphocytes and impair downstream T cell activities. Follow-up studies could explore whether supplementation of PBS with the nutrients found in RPMI singularly, or in small combinations, are sufficient for recovery of deficient T cell activation and functionality.

Intriguingly, we observed increased background expression of CD69 on PBS-washed CD8 T cells, which may be associated with nutrient deprivation during PBMC isolation. The cGAS-STING signaling pathway induces production of type I interferons in response to cellular stress, such as starvation and the absence of the amino acid arginine (Hopfner and Hornung, 2020; Hsu et al., 2021). Previously, researchers have found that type I interferons can partially activate T cells and upregulate CD69 expression in a T cell receptor-independent manner (Sun et al., 1998). Therefore, the upregulation of CD69 expression on unstimulated CD8 T cells may be suggestive of nutritional deprivation during PBS washes, although more research is needed to confirm this hypothesis. We also observed a correlation between the frequency of background $CD69^{+}$ CD8 T cells and baseline numbers of IFNγ-producing cells, suggesting that aberrantly activated CD8 T cells in PBS-washed samples may reduce the sensitivity of the FluoroSpot assay.

Alternatively, background expression of both OX40 and CD137 on CD4 T cells was lowest in RPMI+-processed samples. However, OX40 expression showed increased

upregulation following SARS-CoV-2 stimulation for both methods that used RPMI wash media over PBS and did not differ between the two RPMI methods, while the difference in the upregulation of CD137 between all processing methods was minimal. This suggests that activation of the OX40 pathway may be more dependent on maintained T cell homeostasis during PBMC isolation than the CD137 pathway. Future studies could explore whether other T cell activation markers (such as CD25, CD40L, CD200, HLA-DR, etc.) are more or less susceptible to impaired activation from PBS-induced stress compared with the markers studied here.

While we explored the effect of slower centrifugation speeds and lighter braking during the PBMC isolation process on downstream T cell activities in the RPMI+ method, these changes produced no clear benefits over the RPMI method. Furthermore, slower braking resulted in an additional 1 hour of processing time, which increased the delay between blood collection and cryopreservation. Previously, increased time between collection and freezing has been associated with reduced T cell viability and functionality (Bull et al., 2007; Hope et al., 2021). Thus, we determined the processing method that utilizes RPMI wash media and full centrifugation braking during the wash steps to be the most effective and efficient of the three methods studied.

Our data has limitations. First, the enhancement of T cell responses when using RPMI wash media was not universal, and thus genetic differences may affect an individual's ability to tolerate PBS-induced stress on T cells. Further, we observed trends in our data that may have shown significance given larger sample numbers. Thus, validation of our conclusions in a larger, more diverse cohort is needed. Next, the AIM assay was run without replicates due to limitations of blood collection volume and the number of conditions per sample. Finally, while we used SARS-CoV-2-specific T cell responses following COVID-19 vaccination as a model, the beneficial effects of RPMI media during processing should be validated for other rare antigen-

specific T cell populations. Results may also differ in other settings of immunity, such as following acute infection or in immunocompromised individuals.

5. Conclusions

This study provides one of the first published comparisons of different wash media types and centrifugation settings during PBMC isolation on downstream T cell activation and functionality. We found that RPMI-washed samples showed enhanced detection of SARS-CoV-2-specific T cells over PBS-washed samples through maximized detection of antigen-specific T cell responses and decreased background T cell activation. However, slower centrifugation speeds and lighter braking did not further improve T cell responses, while also significantly lengthening the time from blood collection to cryopreservation. Thus, the use of RPMI wash media and full centrifugation braking during PBMC isolation proved most effective and efficient. Future studies should seek to identify the specific pathways involved in RPMI-mediated T cell enhancement in an effort to further optimize T cell performance in functional assays and improve the reproducibility of these assays between laboratories.

6. Acknowledgements

We would like to thank the study participants for their time and donations, and we would also like to acknowledge additional Pannaraj Lab staff members, Athena Thomassian, Laura Hernandez, Lauren Turner, Shirley Mendieta, and Carolyn Jennifer Marentes Ruiz for help with sample collection and/or manuscript review.

7. Funding

This work was supported by the National Institutes of Health 1 R01 AI173194.

8. References

Bull, M., Lee, D., Stucky, J., Chiu, Y.-L., Rubin, A., Horton, H., McElrath, M.J., 2007. Defining blood processing parameters for optimal detection of cryopreserved antigen-specific responses for HIV vaccine trials. J. Immunol. Methods 322, 57–69. https://doi.org/10.1016/j.jim.2007.02.003

Carr, E.L., Kelman, A., Wu, G.S., Gopaul, R., Senkevitch, E., Aghvanyan, A., Turay, A.M., Frauwirth, K.A., 2010. Glutamine Uptake and Metabolism Are Coordinately Regulated by ERK/MAPK During T Lymphocyte Activation. J. Immunol. 185, 1037–1044. https://doi.org/10.4049/jimmunol.0903586

Cytiva, 2020. HyClone Classical Media Formulation - RPMI-1640 Medium - Liquid Media.

Dan, J.M., Mateus, J., Kato, Y., Hastie, K.M., Yu, E.D., Faliti, C.E., Grifoni, A., Ramirez, S.I., Haupt, S., Frazier, A., Nakao, C., Rayaprolu, V., Rawlings, S.A., Peters, B., Krammer, F., Simon, V., Saphire, E.O., Smith, D.M., Weiskopf, D., Sette, A., Crotty, S., 2021. Immunological memory to SARS-CoV-2 assessed for up to 8 months after infection. Science 371, eabf4063. https://doi.org/10.1126/science.abf4063

Gautam, A., Donohue, D., Hoke, A., Miller, S.A., Srinivasan, S., Sowe, B., Detwiler, L., Lynch, J., Levangie, M., Hammamieh, R., Jett, M., 2019. Investigating gene expression profiles of whole blood and peripheral blood mononuclear cells using multiple collection and processing methods. PloS One 14, e0225137. https://doi.org/10.1371/journal.pone.0225137

Goel, R.R., Painter, M.M., Apostolidis, S.A., Mathew, D., Meng, W., Rosenfeld, A.M., Lundgreen, K.A., Reynaldi, A., Khoury, D.S., Pattekar, A., Gouma, S., Kuri-Cervantes, L., Hicks, P., Dysinger, S., Hicks, A., Sharma, H., Herring, S., Korte, S., Baxter, A.E., Oldridge, D.A., Giles, J.R., Weirick, M.E., McAllister, C.M., Awofolaju, M., Tanenbaum, N., Drapeau, E.M., Dougherty, J., Long, S., D'Andrea, K., Hamilton, J.T., McLaughlin, M., Williams, J.C., Adamski, S., Kuthuru, O., The UPenn COVID Processing Unit, Frank,

I., Betts, M.R., Vella, L.A., Grifoni, A., Weiskopf, D., Sette, A., Hensley, S.E., Davenport, M.P., Bates, P., Luning Prak, E.T., Greenplate, A.R., Wherry, E.J., 2021. mRNA vaccines induce durable immune memory to SARS-CoV-2 and variants of concern. Science 374, abm0829. https://doi.org/10.1126/science.abm0829

Higdon, L.E., Lee, K., Tang, Q., Maltzman, J.S., 2016. Virtual Global Transplant Laboratory Standard Operating Procedures for Blood Collection, PBMC Isolation, and Storage. Transplant. Direct 2, e101. https://doi.org/10.1097/TXD.0000000000000613

Hope, C.M., Huynh, D., Wong, Y.Y., Oakey, H., Perkins, G.B., Nguyen, T., Binkowski, S., Bui, M., Choo, A.Y.L., Gibson, E., Huang, D., Kim, K.W., Ngu, K., Rawlinson, W.D., Sadlon, T., Couper, J.J., Penno, M.A.S., Barry, S.C., On Behalf Of The Endia Study Group, null, 2021. Optimization of Blood Handling and Peripheral Blood Mononuclear Cell Cryopreservation of Low Cell Number Samples. Int. J. Mol. Sci. 22, 9129. https://doi.org/10.3390/ijms22179129

Hope, H.C., Salmond, R.J., 2021. The Role of Non-essential Amino Acids in T Cell Function and Anti-tumour Immunity. Arch. Immunol. Ther. Exp. (Warsz.) 69, 29. https://doi.org/10.1007/s00005-021-00633-6

Hopfner, K.-P., Hornung, V., 2020. Molecular mechanisms and cellular functions of cGAS–STING signalling. Nat. Rev. Mol. Cell Biol. 21, 501–521. https://doi.org/10.1038/s41580-020-0244-x

Hsu, S.-C., Chen, C.-L., Cheng, M.-L., Chu, C.-Y., Changou, C.A., Yu, Y.-L., Yeh, S.-D., Kuo, T.-C., Kuo, C.-C., Chuu, C.-P., Li, C.-F., Wang, L.-H., Chen, H.-W., Yen, Y., Ann, D.K., Wang, H.-J., Kung, H.-J., 2021. Arginine starvation elicits chromatin leakage and cGAS-STING activation via epigenetic silencing of metabolic and DNA-repair genes. Theranostics 11, 7527–7545. https://doi.org/10.7150/thno.54695

Jacobs, S.R., 2009. The Role of Glucose Metabolism in T Cell Stimulation and Homeostasis (Dissertation). Duke University.

Janetzki, S., Britten, C.M., Kalos, M., Levitsky, H.I., Maecker, H.T., Melief, C.J.M., Old, L.J., Romero, P., Hoos, A., Davis, M.M., 2009. “MIATA”—Minimal Information about T Cell Assays. Immunity 31, 527–528. https://doi.org/10.1016/j.immuni.2009.09.007

Kemp, T., Richards, A.C., Hope, D., Pinto, L., 2020. Isolation and Cryopreservation of PBMC (NCI SeroNet Guidance Document) (Version 2.0). Frederick National Laboratory for Cancer Research.

Mallone, R., Mannering, S.I., Brooks-Worrell, B.M., Durinovic-Belló, I., Cilio, C.M., Wong, F.S., Schloot, N.C., T-Cell Workshop Committee, Immunology of Diabetes Society, 2011. Isolation and preservation of peripheral blood mononuclear cells for analysis of islet antigen-reactive T cell responses: position statement of the T-Cell Workshop Committee of the Immunology of Diabetes Society. Clin. Exp. Immunol. 163, 33–49. https://doi.org/10.1111/j.1365-2249.2010.04272.x

Mateus, J., Grifoni, A., Tarke, A., Sidney, J., Ramirez, S.I., Dan, J.M., Burger, Z.C., Rawlings, S.A., Smith, D.M., Phillips, E., Mallal, S., Lammers, M., Rubiro, P., Quiambao, L., Sutherland, A., Yu, E.D., da Silva Antunes, R., Greenbaum, J., Frazier, A., Markmann, A.J., Premkumar, L., de Silva, A., Peters, B., Crotty, S., Sette, A., Weiskopf, D., 2020. Selective and cross-reactive SARS-CoV-2 T cell epitopes in unexposed humans. Science 370, 89–94. https://doi.org/10.1126/science.abd3871

Naranbhai, V., Nathan, A., Kaseke, C., Berrios, C., Khatri, A., Choi, S., Getz, M.A., Tano-Menka, R., Ofoman, O., Gayton, A., Senjobe, F., Zhao, Z., St Denis, K.J., Lam, E.C., Carrington, M., Garcia-Beltran, W.F., Balazs, A.B., Walker, B.D., Iafrate, A.J., Gaiha, G.D., 2022. T cell reactivity to the SARS-CoV-2 Omicron variant is preserved in most but not all individuals. Cell 185, 1041-1051.e6. https://doi.org/10.1016/j.cell.2022.01.029

Newsholme, P., 2001. Why is L-glutamine metabolism important to cells of the immune system in health, postinjury, surgery or infection? J. Nutr. 131, 2515S–22S; discussion 2523S-4S. https://doi.org/10.1093/jn/131.9.2515S

Painter, M.M., Mathew, D., Goel, R.R., Apostolidis, S.A., Pattekar, A., Kuthuru, O., Baxter, A.E., Herati, R.S., Oldridge, D.A., Gouma, S., Hicks, P., Dysinger, S., Lundgreen, K.A., Kuri-Cervantes, L., Adamski, S., Hicks, A., Korte, S., Giles, J.R., Weirick, M.E., McAllister, C.M., Dougherty, J., Long, S., D'Andrea, K., Hamilton, J.T., Betts, M.R., Bates, P., Hensley, S.E., Grifoni, A., Weiskopf, D., Sette, A., Greenplate, A.R., Wherry, E.J., 2021. Rapid induction of antigen-specific CD4+ T cells is associated with coordinated humoral and cellular immunity to SARS-CoV-2 mRNA vaccination. Immunity 54, 2133-2142.e3. https://doi.org/10.1016/j.immuni.2021.08.001

Palmer, C.S., Ostrowski, M., Balderson, B., Christian, N., Crowe, S.M., 2015. Glucose Metabolism Regulates T Cell Activation, Differentiation, and Functions. Front. Immunol. 6.

Protocol No. DMID-OCRR-SOP-002, 2021. Standard Operating Procedure: Peripheral Blood Mononuclear Cells (PBMC) and Associated Plasma Collection (Version 6.0). National Institute of Allergy and Infectious Diseases, Division of Microbiology and Infectious Diseases.

Rydyznski Moderbacher, C., Ramirez, S.I., Dan, J.M., Grifoni, A., Hastie, K.M., Weiskopf, D., Belanger, S., Abbott, R.K., Kim, Christina, Choi, J., Kato, Y., Crotty, E.G., Kim, Cheryl, Rawlings, S.A., Mateus, J., Tse, L.P.V., Frazier, A., Baric, R., Peters, B., Greenbaum, J., Ollmann Saphire, E., Smith, D.M., Sette, A., Crotty, S., 2020. Antigen-Specific Adaptive Immunity to SARS-CoV-2 in Acute COVID-19 and Associations with Age and Disease Severity. Cell 183, 996-1012.e19. https://doi.org/10.1016/j.cell.2020.09.038

Sun, S., Zhang, X., Tough, D.F., Sprent, J., 1998. Type I Interferon-mediated Stimulation of T Cells by CpG DNA. J. Exp. Med. 188, 2335–2342.

Tarke, A., Sidney, J., Methot, N., Yu, E.D., Zhang, Y., Dan, J.M., Goodwin, B., Rubiro, P., Sutherland, A., Wang, E., Frazier, A., Ramirez, S.I., Rawlings, S.A., Smith, D.M., da Silva Antunes, R., Peters, B., Scheuermann, R.H., Weiskopf, D., Crotty, S., Grifoni, A.,

Sette, A., 2021. Impact of SARS-CoV-2 variants on the total CD4+ and CD8+ T cell reactivity in infected or vaccinated individuals. Cell Rep. Med. 2, 100355. https://doi.org/10.1016/j.xcrm.2021.100355

van der Windt, G.J.W., Pearce, E.L., 2012. Metabolic switching and fuel choice during T-cell differentiation and memory development. Immunol. Rev. 249, 27–42. https://doi.org/10.1111/j.1600-065X.2012.01150.x

Wasinski, F., Gregnani, M.F., Ornellas, F.H., Bacurau, A.V.N., Câmara, N.O., Araujo, R.C., Bacurau, R.F., 2014. Lymphocyte Glucose and Glutamine Metabolism as Targets of the Anti-Inflammatory and Immunomodulatory Effects of Exercise. Mediators Inflamm. 2014, e326803. https://doi.org/10.1155/2014/326803

9. Tables

Table 1. Participant demographics and clinical characteristics.

Characteristic	**N (%)** (n=26)
Sex	
Male	13 (50)
Female	13 (50)
Age at blood collection	
18-29	14 (54)
30-54	11 (42)
55+	1 (4)
Ethnicity	
Hispanic/Latino	9 (32)
Non-Hispanic/Latino	17 (65)
Race	
Asian	13 (50)
White	11 (42)
Other	1 (4)
Multiple	1 (4)
Primary series vaccine type (manufacturer)	
BNT162b2 (Pfizer-BioNTech)	19 (73)
mRNA-1273 (Moderna)	5 (19)
Ad26.COV2.S (Johnson & Johnson)	2 (8)
Booster vaccine type (manufacturer)	
BNT162b2, Monovalent (Pfizer-BioNTech)	19 (73)
mRNA-1273, Monovalent (Moderna)	5 (19)
mRNA-1273.214, Bivalent (Moderna)	2 (8)
None	1 (4)
Previous SARS-CoV-2 infection	
Yes	12 (46)
No/Unknown	14 (54)

Table 2. Differences between the PBS, RPMI, and RPMI+ processing methods

	PBS	RPMI	RPMI+
Wash media type	PBS, pH 7.4	RPMI-1640 + 2.05 mM L-glutamine	RPMI-1640 + 2.05 mM L-glutamine
Plasma isolation			
Blood diluted in wash media?	No	No	Yes
Centrifugation speed, time (deceleration setting)	1200xG, 10 min (deceleration: 9)	1200xG, 10 min (deceleration: 9)	800xG, 10 min (deceleration: 0)
Buffy coat separation			
Separation method	Leucosep tube + Ficoll-Paque Plus	Leucosep tube + Ficoll-Paque Plus	Ficoll-Paque Plus overlay method
Centrifugation speed, time (deceleration setting)	1000xG, 10 min (deceleration: 0)	1000xG, 10 min (deceleration: 0)	800xG, 25 min (deceleration: 0)
Wash steps			
Number of wash steps	3	3	2
Centrifugation speed, time (deceleration setting)	400xG, 10 min (deceleration: 9)	400xG, 10 min (deceleration: 9)	400xG, 10 min (deceleration: 4)
Final spin before freezing			
Centrifugation speed, time (deceleration setting)	400xG, 10 min (deceleration: 9)	400xG, 10 min (deceleration: 9)	200xG, 10 min (deceleration: 0)
Average processing time	1.5 hr	1.5 hr	2.5 hr

10. Figures

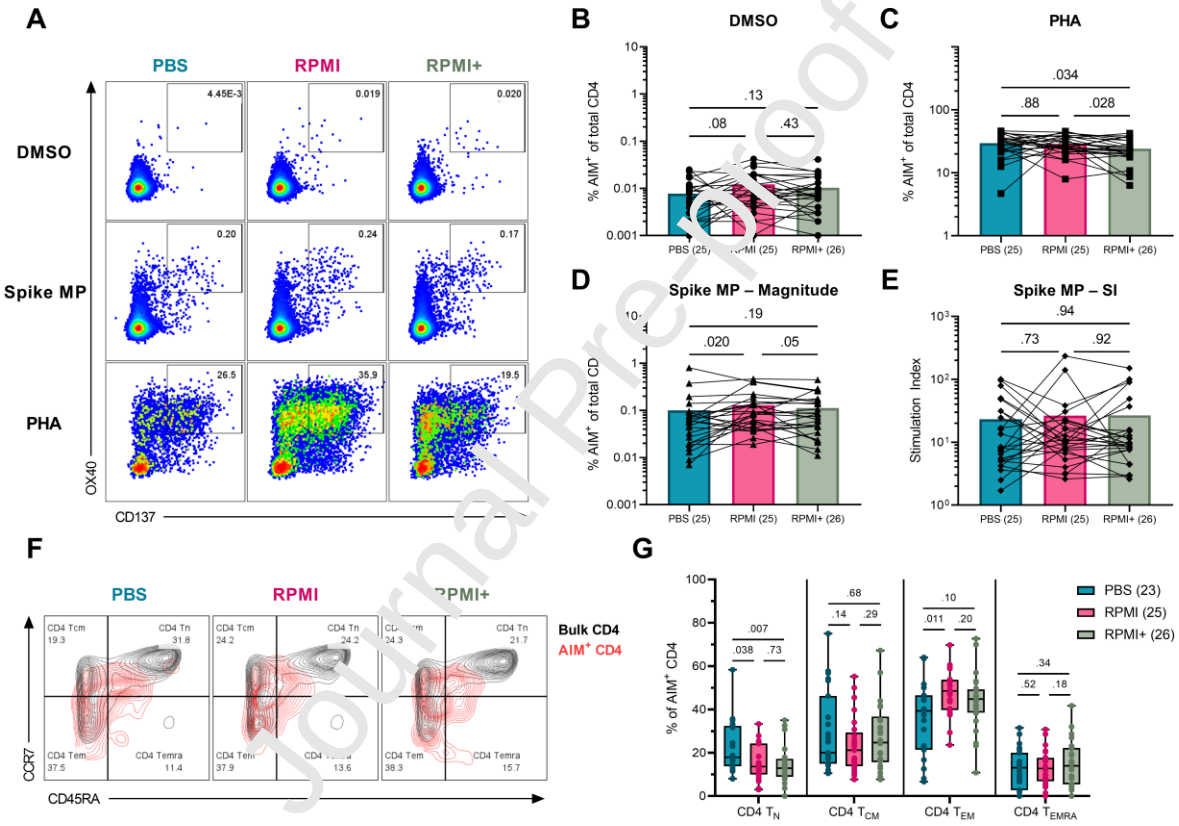

Figure 1. Comparison of AIM$^+$ CD4 T cell responses to the SARS-CoV-2 spike protein between the PBS, RPMI, and RPMI+ processing methods. (A) A representation of the differences in AIM$^+$ CD4 T cells, defined as OX40$^+$CD137$^+$, between the different processing methods for each stimulation condition is presented. Numbers are the percentage AIM$^+$ of total CD4 T cells. Comparisons of AIM$^+$ CD4 T cells between processing methods are shown for the **(B)** DMSO- and **(C)** PHA-stimulated conditions. The **(D)** magnitudes and **(E)** stimulation indices

of Spike MP-stimulated AIM$^+$ CD4 T cells are also compared between processing methods. All bars are at the median of each group. **(F)** An example of the differences in memory subsets of AIM$^+$ CD4 T cells by processing method is shown. Numbers are the percentage of each subset in AIM$^+$ CD4 T cells; black color corresponds to the bulk CD4 T cell population while red corresponds to the AIM$^+$ CD4 population. **(G)** Changes in each AIM$^+$ CD4 memory subset are compared between the different processing methods. Boxes are at the median and 1st and 3rd quartiles, and whiskers are at the minimum and maximum. Statistical differences between groups were calculated using the Wilcoxon signed-rank test. Data is from 8 independent experiments.

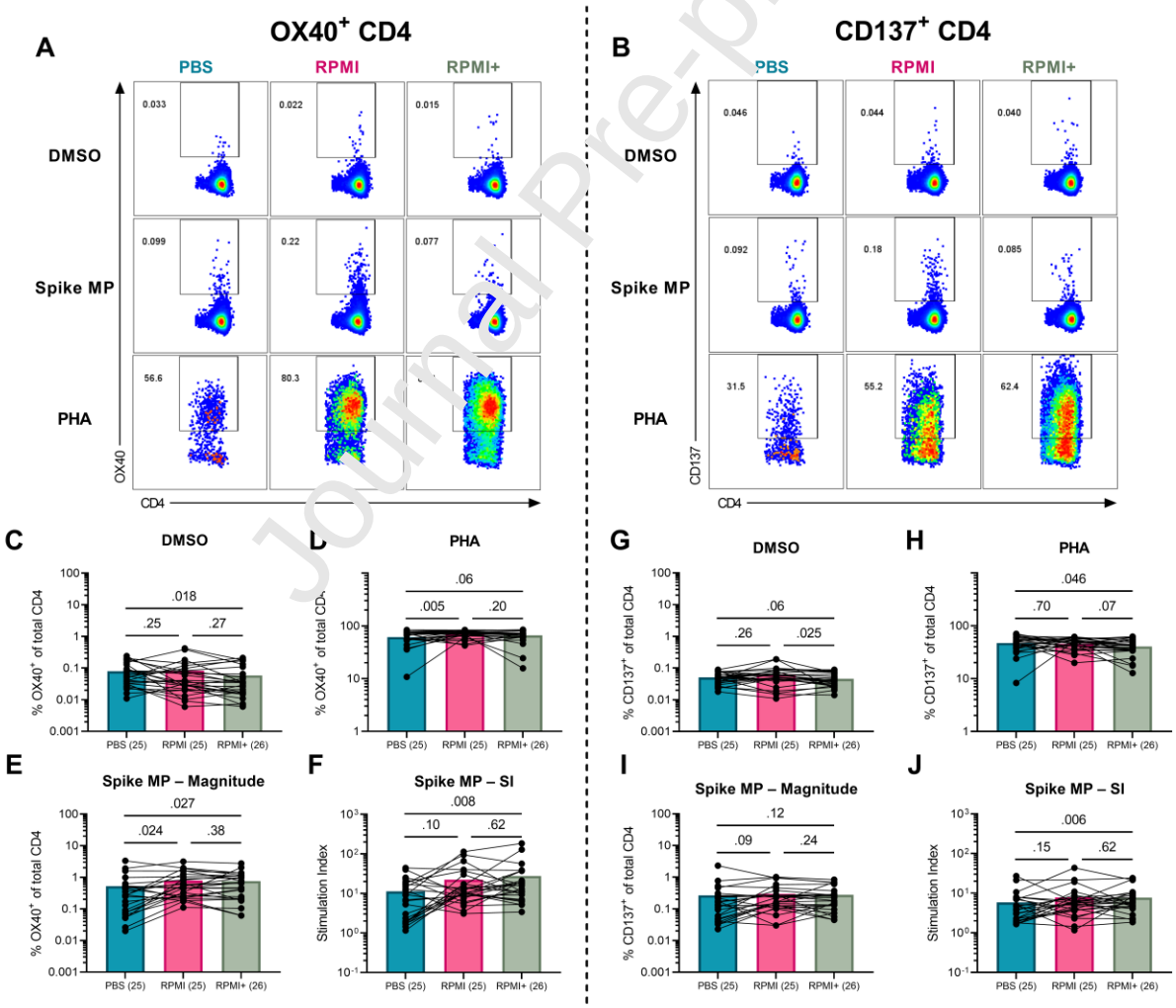

Figure 2. Differences in the single expression of OX40 or CD137 on CD4 T cells between the PBS, RPMI, and RPMI+ processing methods. Representative samples of singular **(A)** OX40 or **(B)** CD137 expression on CD4 T cells following DMSO, Spike MP, and PHA stimulation for each processing method are shown. Numbers are percentage $OX40^+$ or $CD137^+$ of total CD4 T cells. Comparisons of the proportions of $OX40^+$ CD4 T cells between processing methods for the **(C)** DMSO- and **(D)** PHA-stimulated conditions are presented, followed by the **(E)** magnitudes and **(F)** stimulation indices of OX40 expression following Spike MP stimulation. For $CD137^+$ CD4 T cells, proportions are compared between processing methods for the **(G)** DMSO- and **(H)** PHA-stimulated conditions, as well as for **(I)** the magnitudes and **(J)** stimulation indices of CD137 expression following Spike MP stimulation. All bars are at the median. Statistical differences between groups were calculated using the Wilcoxon signed-rank test. Data is from 8 independent experiments.

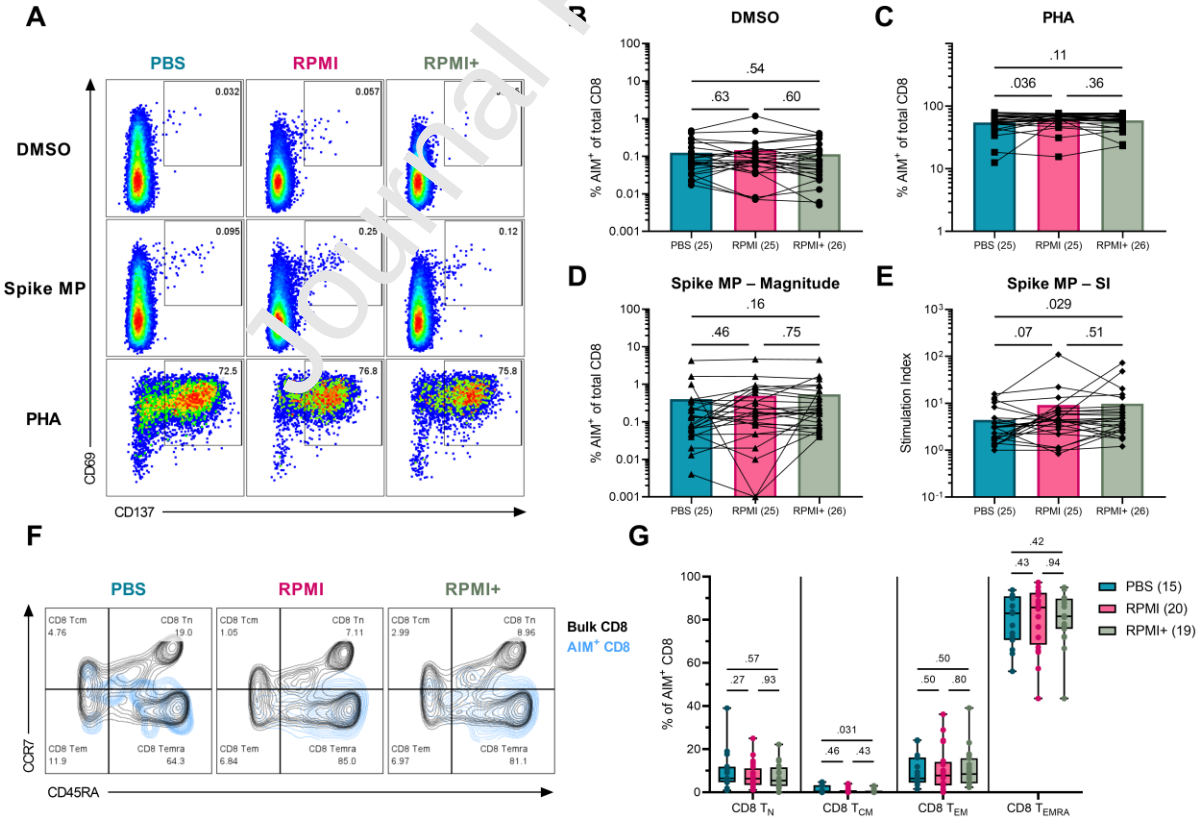

Figure 3. Comparison of AIM$^+$ CD8 T cell responses to the SARS-CoV-2 spike protein between the PBS, RPMI, and RPMI+ processing methods. AIM$^+$ CD8 T cells were defined as CD69$^+$CD137$^+$, and **(A)** an example of differences in the background, spike-specific, and PHA-stimulated AIM$^+$ CD8 responses between the different processing methods is presented. Numbers are the percentage AIM$^+$ of total CD8 T cells. Comparisons of the proportions of AIM$^+$ CD8 T cells between processing methods are shown for the **(B)** DMSO- and **(C)** PHA-stimulated conditions. The **(D)** magnitudes and **(E)** stimulation indices of Spike MP-stimulated AIM$^+$ CD8 T cells are also compared between processing methods. All bars are at the median. **(F)** An example of the differences in AIM$^+$ CD8 T cell memory subsets by processing method is shown. Numbers are the percentage of each subset in AIM$^+$ CD8 T cells; black color corresponds to the bulk CD8 T cell population while blue corresponds to the AIM$^+$ CD8 population. **(G)** The shifts in each AIM$^+$ CD8 memory subset between the different processing methods are presented. Boxes represent the median and 1st and 3rd quartiles while whiskers are at the minimum and maximum. Statistical differences between groups were calculated using the Wilcoxon signed-rank test. Data is from 8 independent experiments.

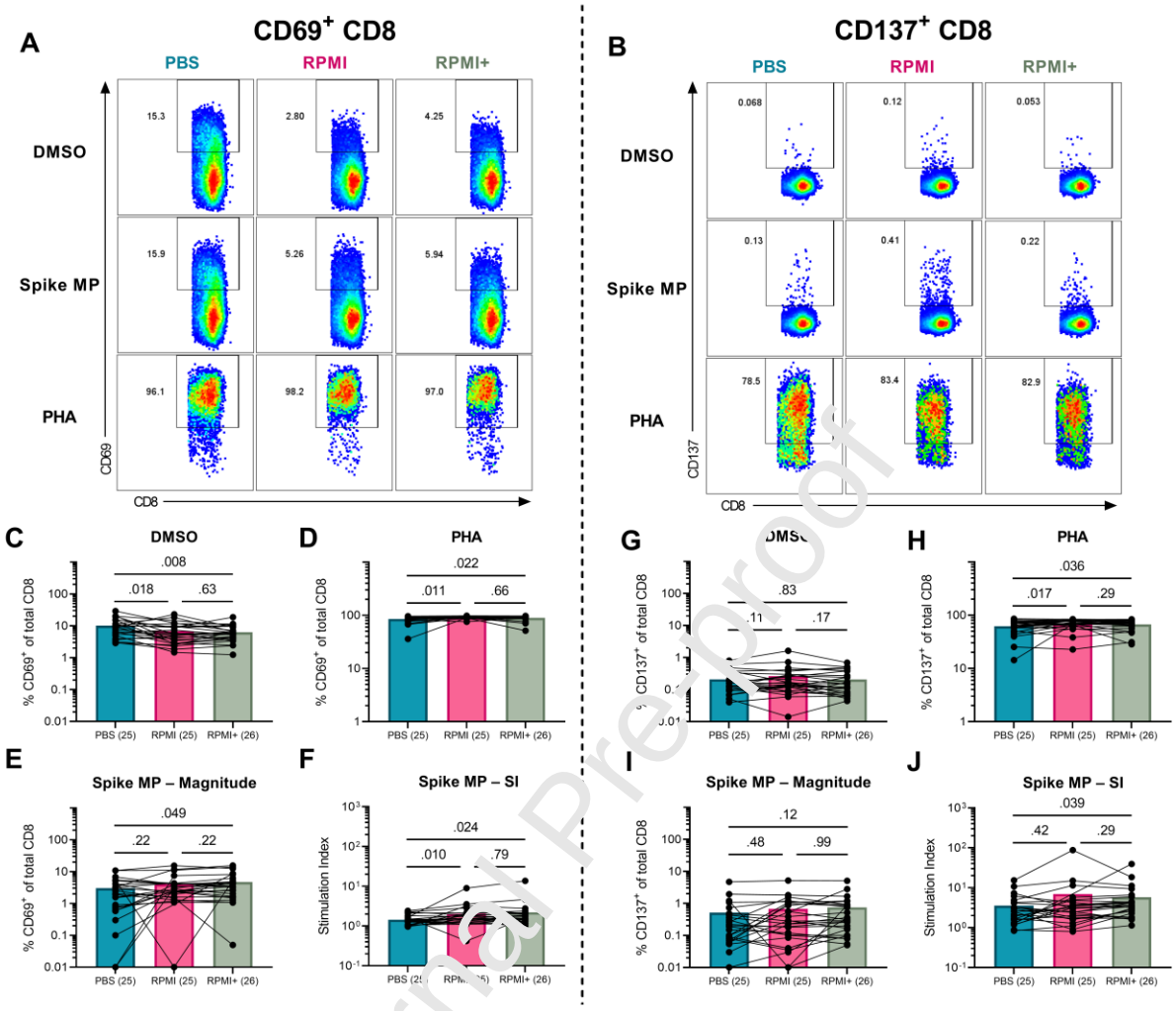

Figure 4. Differences in the single expression of CD69 or CD137 on CD8 T cells between the PBS, RPMI, and RPMI+ processing methods. Representative samples of singular **(A)** CD69 or **(B)** CD137 expression on CD8 T cells following DMSO, Spike MP, and PHA stimulation compared between the different processing methods are shown. Numbers are the percentage CD69$^+$ or CD137$^+$ of total CD8 T cells. Comparisons of CD69$^+$ CD8 T cells between processing methods are presented for the **(C)** DMSO- and **(D)** PHA-stimulated conditions. The **(E)** magnitudes and **(F)** stimulation indices of Spike MP-induced CD69 expression are also compared between processing methods. For CD137$^+$ CD8 T cells, differences in CD137 expression between processing methods for the **(G)** DMSO- and **(H)** PHA-stimulated conditions

and changes in the **(I)** magnitudes and **(J)** stimulation indices following Spike MP stimulation are presented. All bars at the median. Statistical differences between groups were calculated using the Wilcoxon signed-rank test. Data is from 8 independent experiments.

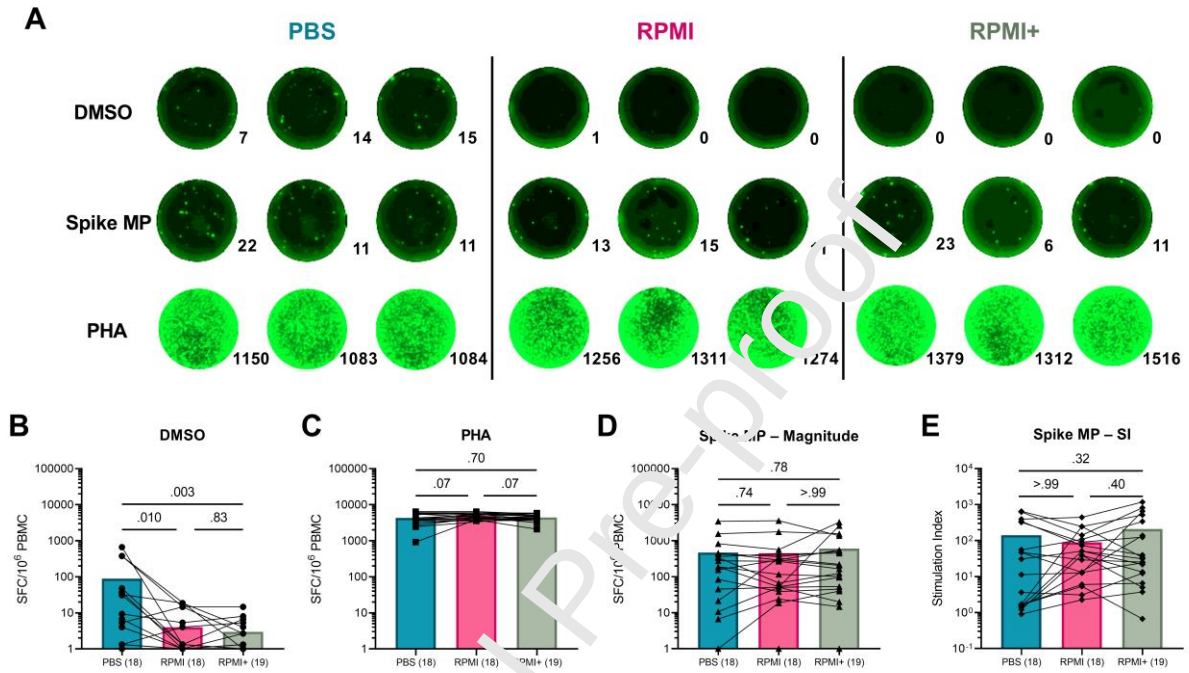

Figure 5. Comparison of SARS-CoV-2 spike-induced IFNγ production by T cells processed using the PBS, RPMI, and RPMI+ methods. (A) An example of the differences in the numbers of IFNγ spot forming cells (SFC)/2.5x10^5 PBMC for each stimulation condition between processing methods is shown. Numbers to the bottom right of each well are the number of SFC per well. Comparisons in the numbers of IFNγ SFC/10^6 PBMC between the different processing methods are shown for the **(B)** DMSO- and **(C)** PHA-stimulated conditions. The **(D)** magnitudes and **(E)** stimulation indices for IFNγ SFC/10^6 PBMC are compared between processing methods. All bars are at the median. Statistical differences between groups were calculated using the Wilcoxon signed-rank test. All conditions were run in triplicate. Data is from 9 independent experiments.

Supplementary Tables

Supplementary Table 1. Antibodies for AIM T cell assay

Antigen	Fluorophore	Clone	Species	Dilution	Manufacturer	Catalog No.
CD3	BUV395	UCHT1	Mouse	1:50	BD Biosciences	563546
CD4	FITC	SK3	Mouse	1:50	BioLegend	344604
CD8	BV510	SK1	Mouse	1:50	BioLegend	344732
CD14	Pacific Blue	M5E2	Mouse	1:100	BioLegend	301828
CD19	Pacific Blue	HIB19	Mouse	1:100	BioLegend	302232
CD45RA	BV785	HI100	Mouse	1:50	BioLegend	304140
CD56	Pacific Blue	MEM-188	Mouse	1:100	BioLegend	304629
CD69	PE/Cyanine7	FN50	Mouse	1:33	BioLegend	310912
CD134 (OX40)	PE	Ber-ACT35	Mouse	1:33	BioLegend	350004
CD137 (41BB)	APC	4B4-1	Mouse	1:33	BioLegend	309810
CD185 (CXCR5)	Alexa Fluor 700	J252D4	Mouse	1:100	BioLegend	356916
CD197 (CCR7)	PerCP/Cyanine5.5	G043H7	Mouse	1:50	BioLegend	353220
CD279 (PD-1)	PE-Dazzle594	EH12.2H7	Mouse	1:50	BioLegend	329940
Zombie UV Fixable Viability	-	-	-	1:100	BioLegend	423108

Supplementary Figures

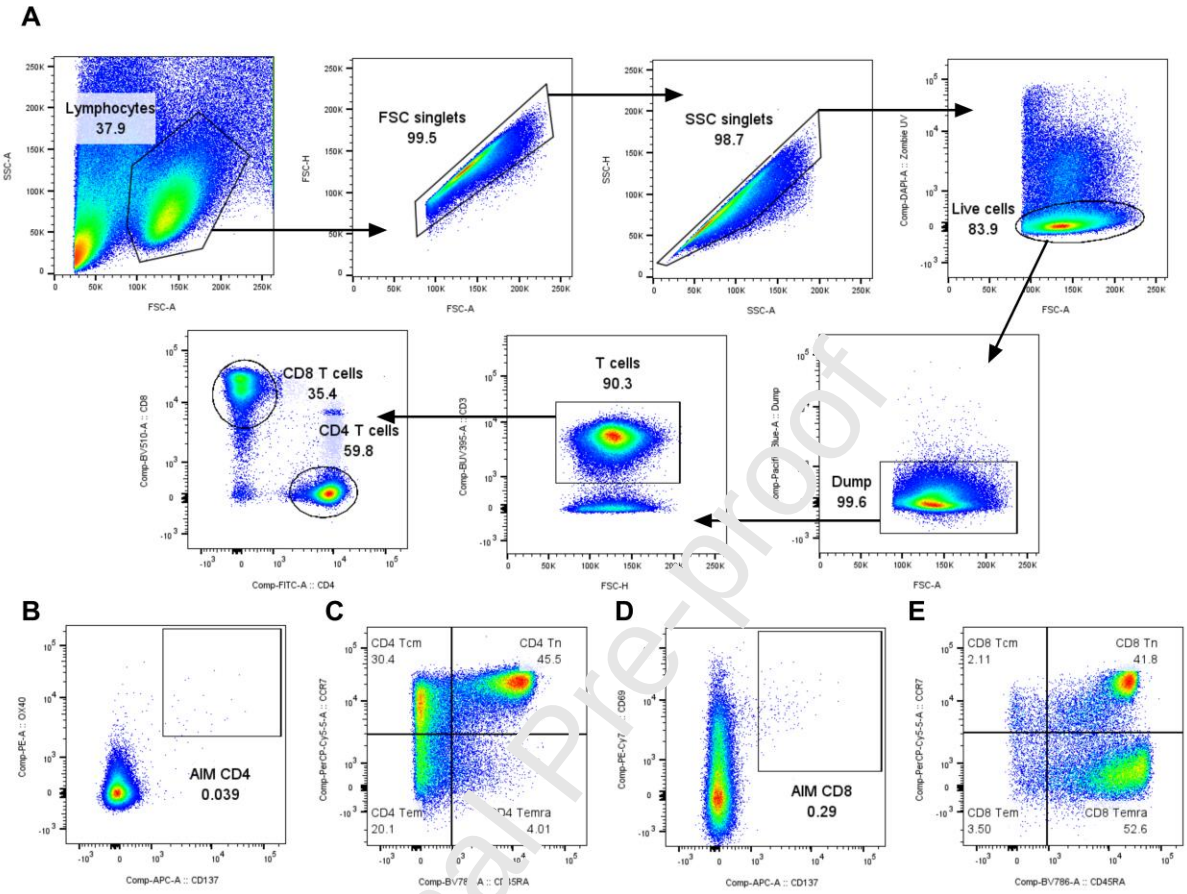

Supplementary Figure 1. Gating strategy for identification of AIM$^+$ CD4 and CD8 T cell populations and memory subsets. (A) Lymphocytes were identified by forward scatter (FSC) and side scatter (SSC). Then singlets were gated on by FSC height and area and SSC height and area. Negative staining for the Zombie UV viability dye, which is detected in the DAPI channel, was used to identify live cells. B cells, monocytes, and NK cells were excluded using a dump channel, and then T cells were positively selected for by CD3 expression. CD4 and CD8 T cells were then identified. **(B)** AIM$^+$ CD4 T cells were defined as OX40$^+$CD137$^+$ and **(C)** memory subsets in bulk CD4 T cells and AIM$^+$ CD4 T cells were identified via differential expression of CCR7 and CD45RA based on fluorescence minus one controls. **(D)** Similarly, AIM$^+$ CD8 T cells were identified as CD69$^+$CD137$^+$ and **(E)** memory subsets were also identified

through CCR7 and CD45RA expression based on fluorescence minus one controls. All numbers refer to percentage of the parent population.

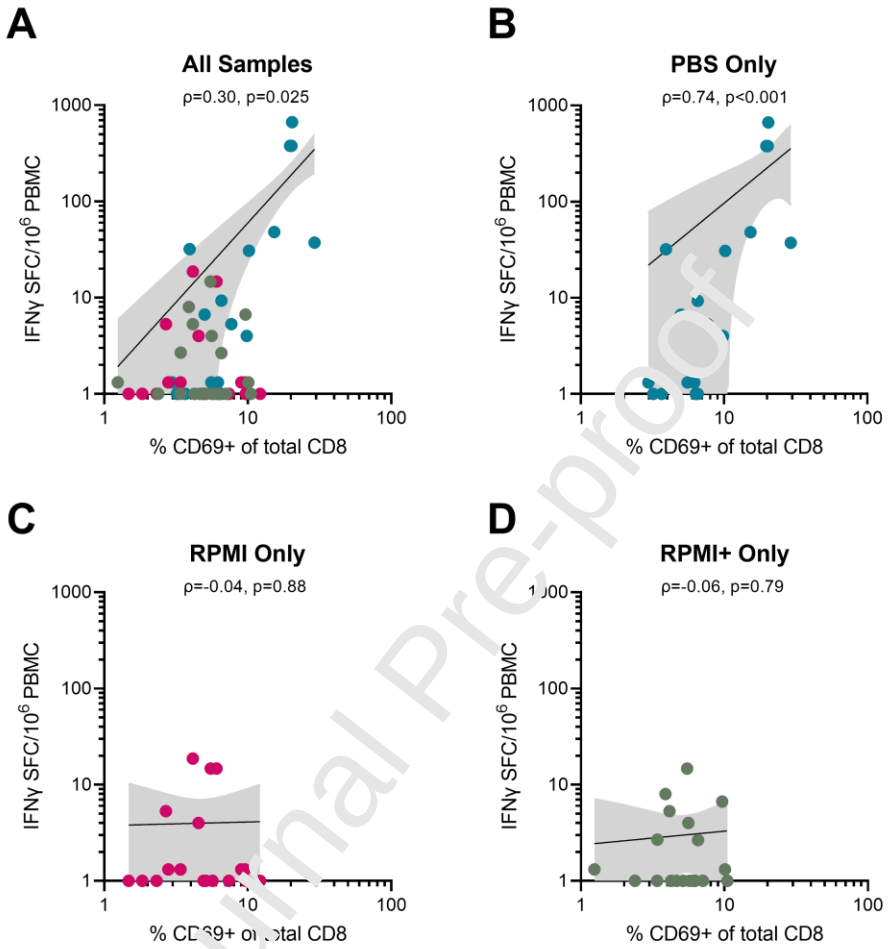

Supplementary Figure 2. Correlations between background IFNγ-producing cells and CD69-expressing CD8 T cells. (A) The association between numbers of IFNγ SFC/10^6 PBMC in the DMSO condition and the corresponding proportion of $CD69^+$ CD8 T cells for the same sample is presented across all processing methods (n=55). The associations between background IFNγ SFC/10^6 PBMC and percentages of $CD69^+$ CD8 T cells are also shown for samples processed with the **(B)** PBS method (n=18), **(C)** RPMI method (n=18), and **(D)** RPMI+ method (n=19) separately. All correlations were calculated using Spearman's correlation coefficient. Lines of best fit were determined using a log-log line nonlinear regression.